Combined carbon photon and hydrogel therapy mediates the synergistic repair of full-thickness skin wounds

Fan Yang[1,2,3,*], Xiuling Zhou[1,*], Sitong Chen[1], Qiuju Li[2], Ronghang Li[2], Chunying Li[1], Chenyu Shi[2,3] and Lanyu Zhu[1]

Abstract

Objective: This study investigated the synergistic repair effects of Prontosan hydrogel and carbon photon therapy in a rat full-thickness wound model.

Methods: The wavelength distribution of the photon source was determined. Dehydration of the Prontosan hydrogel and fibroblast viability were analyzed following exposure to different durations of light exposure at different distances from the source. Indexes of wound healing in a full-thickness rat wound model were then determined in groups ($n = 8$ each) subjected to either no treatment, Prontosan treatment only, carbon photon therapy only, or a combination of the two treatments (synergistic group).

Results: Carbon photon exposure for 15 minutes at a distance of 20 cm from the wound was found to be optimal. Wound healing occurred faster in the synergistic group compared with the control and single-treatment groups. Growth factor secretion, granulation tissue formation, inflammation regulation, collagen deposition, and neovascularization were all higher in the synergistic group.

Conclusions: Prontosan hydrogel combined with carbon photon therapy may provide an optimal environment for wound healing and serve as a novel physical approach to the treatment of wounds. However, the number of animals included in this study was relatively small and a larger study is required to confirm these findings.

[3]Orthopaedic Research Institute of Jilin Province, Changchun, P. R. China

*These authors contributed equally to this work.

[1]School of Nursing, Changchun University of Chinese Medicine, Changchun, P. R. China
[2]Department of Orthopedics, The Second Hospital of Jilin University, Changchun, P. R. China

Corresponding author:
Lanyu Zhu, School of Nursing, Changchun University of Chinese Medicine, Changchun 130117, P. R. China.
Email: zhulanyu2006@126.com

Introduction

Wound healing involves a variety of biological processes including epithelial cell and fibroblast proliferation, revascularization, and wound contraction.[1] Numerous internal and external factors can influence the speed and quality of wound healing, and an inappropriate microenvironment can impede the healing process, leading to chronic wound or scar formation.[2]

Light is a natural treatment with no toxic side effects, and it is remarkably effective in treating various types of pain, trauma, and skin disease.[3] The carbon arc is a broad-spectrum light source that includes visible light, infrared, ultraviolet, and magnetic pulses, and it can exert thermal and photochemical effects. Using carbon photons as a therapeutic approach can exert anti-inflammatory and sterilizing effects on human tissues and can promote tissue metabolism, growth, and circulation in wounds.[4] Recently, carbon photon therapy was shown to promote wound healing in a rat full-thickness wound model by stimulating cell proliferation.[5] However, the warming effect caused by the carbon photons can lead to a dry local wound microenvironment, which is not conducive to wound healing.[6]

Hydrogels comprise three-dimensional networks of hydrophilic polymers, allowing the absorption of water from 10% up to thousands of times their weight until the process reaches an equilibrium state.[7] Hence, hydrogel dressings can provide a moist environment to promote wound closure and may ameliorate the dry local wound microenvironment caused by carbon photon therapy.[8] As a commercial liquid wound dressing, Prontosan hydrogel not only provides a moist wound healing environment but is also beneficial in sealing the wound and reducing infection. This hydrogel destroys the structure of bacterial biofilms by denaturing the bacterial proteins and leading to cell death.[9] However, synergistic treatment comprising Prontosan hydrogel and carbon photon therapy in the acceleration of wound healing has not yet been fully investigated, particularly at the cellular and molecular levels. Therefore, in the present study, our key objective was to investigate their synergistic effect in the treatment of wounds and the underlying mechanisms involved by examining the gross morphology and pathology of a rat wound model.

Materials and Methods

Materials

A carbon photon therapy device to generate carbon light was purchased from Jilin Fengrui Medical Devices Co., Ltd. (Changchun, China). Prontosan wound hydrogel was obtained from B. Braun Medical AG (Sempach, Switzerland), while phosphate-buffered saline (PBS) and 4% paraformaldehyde were purchased from Beijing Solarbio Science & Technology Co., Ltd. (Beijing, China). Antibodies for immunohistochemical analysis were purchased from Abcam PLC (Cambridge, UK). Hematoxylin and eosin (H&E) and Masson trichrome staining kits, the enzyme-linked immunosorbent assay

(ELISA) kits for various growth factors, and 3-(4,5-dimethylthiazol-2-yl)-2,5-diphe-nyltetrazolium bromide (MTT) were purchased from Sigma-Aldrich (St. Louis, MO, USA). Dimethyl sulfoxide (DMSO) was stored over calcium hydride (CaH_2) and purified by vacuum distillation in the presence of CaH_2.

Wavelength analysis and dehydration effects on Prontosan hydrogel

An ARTUS 10 spectrometer (ARUN Technology, Ltd., Crawley, UK) was used to analyze the spectrum of the carbon light emitted by the carbon photon therapy device. Briefly, we first preheated the ARTUS 10 spectrometer for 30 minutes. The carbon photon therapy device was then placed in a darkroom box, and the device was set to emit its light into the optical path of the spectrometer. The light source on the ARTUS 10 spectrometer was changed to the ultraviolet, visible, and infrared regions in sequence. Finally, the spectral information of the light source emitted by the carbon photon therapy device was recorded and its wavelength distribution was obtained. The dehydration effects of carbon photon exposure on Prontosan hydrogel at different distances from the light source and for different durations of exposure were next determined. The carbon photon therapy device was placed at either 5, 10, 20, or 30 cm from the Prontosan hydrogel (1 g, original weight), and the gel ($n = 3$ in each group) was exposed to the light source for different durations (5, 10, 15, 20, or 25 minutes). Following treatment, the residual weight of the hydrogel was determined, and the dehydration rate of the hydrogel was calculated according to the following formula: gel dehydration rate = (original weight − residual weight)/original weight × 100%.

Effect of carbon photon therapy on fibroblast survival in vitro

In vitro cytotoxicity of the carbon photon treatment toward L929 cells (fibroblasts) was assessed with the MTT assay. Briefly, L929 cells were seeded in a 96-well culture plate at a density of 1×10^4 cells per well and incubated in Ham's F-12 medium supplemented with 10% fetal bovine serum, $100.0 \, U \, mL^{-1}$ penicillin, and $100.0 \, \mu g \, mL^{-1}$ streptomycin at 37°C for 24 hours. The carbon photon therapy device was placed at a distance of either 5, 10, 20, or 30 cm from the cell samples, and the cell samples were then subjected to different periods of light exposure comprising either 0 (control group), 5, 10, 15, 20, or 25 minutes ($n = 3$ in each group). The medium was replaced with fresh medium, followed by the addition of 20 μL of MTT ($5.0 \, mg \, mL^{-1}$) to each well. After incubation at 37°C for 4 hours, the precipitated formazan was dissolved in 200.0 mL of DMSO, and the absorbance value at 490 nm was measured on a microplate reader (ELx680, BioTek Instruments, Inc., Winooski, VT, USA). All measurements were performed in triplicate. Cell viability (%) was calculated according to the followed equation: viability (%) = $(A_{sample})/(A_{control}) \times 100\%$, where A_{sample} and $A_{control}$ were the absorbance values of the sample and control wells, respectively.

Preparation of the wound model

The animal procedures used in this study were approved by the Jilin University Institutional Animal Care and Use Committee (Approval No. SY201904023). Sprague-Dawley rats ($n = 32$ with 16 females and 16 males; average weight, 220 ± 30 g) were used for this investigation. Before and during the experiments, all rats were housed in individual cages with a 12-hour light–dark cycle at the appropriate temperature and humidity and given free

access to standard rodent chow and water. Rats were anesthetized by the intraperitoneal injection of 10% chloral hydrate solution (0.3 mL/100 g), then the back hair was removed and the skin was disinfected using 75% alcohol. Next, a full-thickness skin wound (diameter = 1 cm) was generated with a punch biopsy, and sterile gauze was used to stop the bleeding. Postoperatively, rats were allowed free movement in a separate cage.

Treatments applied to the wound model

Treatments were applied to each wound immediately after wounding and then once every 2 days. The rats were divided into four treatment groups: (1) the BLA group (BLA, $n = 8$) received routine wound care, using a conventional gauze sponge; (2) the GEL group (GEL, $n = 8$) received Prontosan hydrogel dressing (200 µL); (3) the CPT group (CPT, $n = 8$) received a single application of carbon photon therapy for 15 minutes with the light source positioned 20 cm from the wound (based on previous experimental results); (4) the GEL combined with CPT group (G&C, $n = 8$) received both the Prontosan hydrogel and carbon photon treatments. For carbon photon therapy, each rat was placed in a small box with smooth walls. The top of the box was closed with a wire mesh (this did not affect the light treatment). The rats could move freely at the bottom of the box. The carbon photon therapy device was placed on top of the box and the light was applied 20 cm from the back of the rat for the duration of the carbon photon treatment.

Wound area analysis and sample management

The wound area measured on day 0 was defined as the baseline area, and the wound size was recorded once every 2 days using a digital camera until the animals were sacrificed. The percentage area of the wound defect was then carefully determined using ImageJ software (U. S. National Institutes of Health, Bethesda, Maryland, USA) as previously described with the following formula:[10]

Percentage area of wound defect (%) = $S_n/S_o \times 100\%$, where S_o is the baseline area and S_n is the wound area at n days post wounding.

Animals from each group were randomly sacrificed using an overdose of sodium pentobarbital (100 mg/kg) administered intravenously at 8 days ($n = 4$) or 16 days ($n = 4$) after wounding. Samples of the tissue in the wound area were harvested, along with at least 0.2 cm of surrounding healthy tissue, at the depth of the muscle fascia. These samples were divided into two aliquots each, with the first set being used for histological examination and the other set being used for determining the concentrations of various growth factors related to wound regeneration.

Measurement of growth factor concentrations in wound tissue

Tissue samples were homogenized on ice in PBS (0.01 M, pH 7.4, containing protease inhibitors) at a ratio of 100 mg of tissue per 1 mL of PBS, centrifuged at 1,250 $\times g$ for 20 minutes, and the supernatants were collected. Finally, the concentrations of various growth factors in the wound tissue, such as transforming growth factor-β1 (TGF-β1), vascular endothelial growth factor (VEGF), and basic fibroblast growth factor (bFGF), were verified by ELISA.

Histological and immunohistochemical analysis

For histological and immunohistochemical analysis, samples were fixed in 4% (w/v) paraformaldehyde for 24 hours, paraffin-embedded, and cut into 6-µm sections.

First, samples were stained with H&E and Masson trichrome according to the manufacturer's protocols. The number of inflammatory cells was determined by counting three randomly selected areas within the H&E-stained image. Further, wound subepithelial dermal matrix maturity was measured by two trained clinicians, with granulation tissue, inflammation, fibroblasts, collagen deposition, and neovascularization included in the scoring system.[11] Additionally, immunostaining of keratin 14 (K14) and platelet endothelial cell adhesion molecule (also known as cluster of differentiation 31, CD31) was conducted to evaluate the presence of blood vessels and cytokeratin, respectively. Blood vessels in regenerated tissue samples were also quantified, as described previously.[12]

Statistical Analysis

Data are expressed as the mean $\pm$ standard deviation (SD) and the independent samples t-test was used to analyze differences between groups. *P* values < 0.05 were considered statistically significant.

Results and Discussion

Wavelength distribution of the carbon light source

Light therapy is a promising drug-free approach for the repair of damaged tissue, and it has been successfully applied in the clinic.[13] Here, the wavelength distribution of the carbon light source used in this study was obtained by spectrometry (Figure 1). This verified that the carbon light included near-ultraviolet light (350–400 nm) and visible light of various wavelengths, with a particularly large amount of purple light (400–450 nm) and red light (600–660 nm). Near-ultraviolet and purple light appear to enhance immunity and exert a bactericidal effect.[14] However, red light has strong penetrating power, with a deep warming effect that promotes blood circulation and stimulates local blood vessel regeneration.[15]
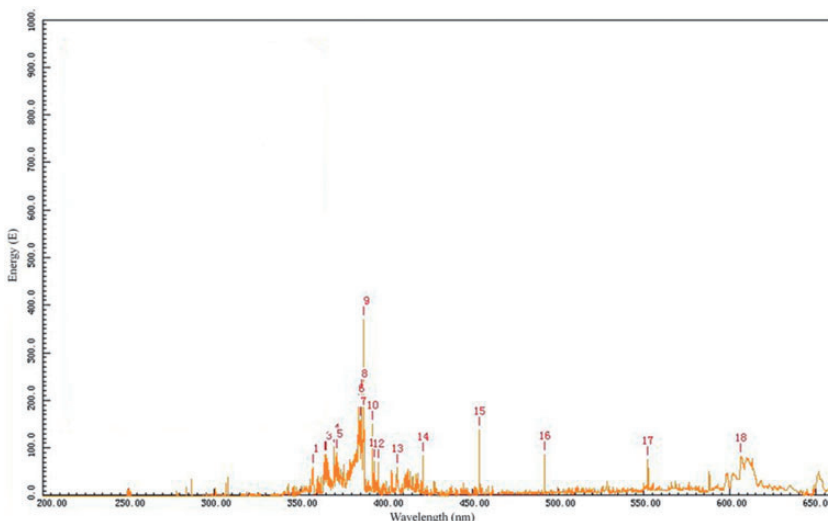

Figure 1. Wavelength distributions of carbon light source as determined by spectrometry between 200 and 660 nm.

Gel dehydration and cell viability affected by duration of light exposure and distance from source

The warming effect of light therapy can cause a dry local microenvironment within the wound, which is not conducive to wound healing.[6] However, hydrogels maintain a moist wound environment, which can mitigate the warming effect of light therapy to a certain degree.[16,17] Hence, it was essential to determine the dehydration effect of carbon photon therapy on hydrogel dehydration and cell viability.

A series of predetermined indexes were used to investigate the effect of carbon photon therapy on hydrogel dehydration (Figure 2a). The degree of hydrogel dehydration clearly increased with increasing duration of light exposure. Further, the distance between the light source and the hydrogel also affected hydrogel dehydration. The *in vitro* cytotoxicity of carbon photons toward fibroblasts was next assessed using different lighting exposure times and distances from the source (Figure 2b). The fibroblasts retained high viability ($>85\%$) when subjected to distant lighting and short-term treatment. However, significant cell death occurred when the distance from the light source was shortened to less than 20 cm ($P < 0.05$) when maintaining the same light exposure time. In addition, light
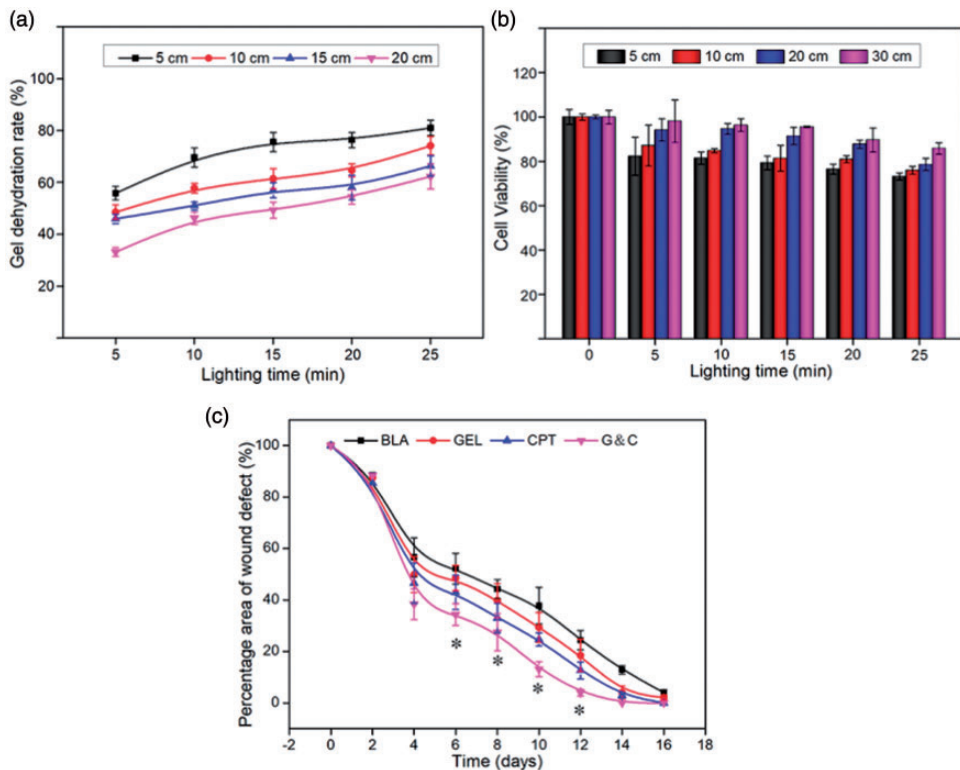

Figure 2. Gel dehydration rate of Prontosan hydrogel (a) and cell viability of fibroblasts (b) when subjected to different periods of light exposure at different distances from the light source. The percentage area of the wound defect (c) at different time points post-wounding in the four treatment groups. Data represent the mean $\pm$ SD, $n = 4$, *$P < 0.05$.

exposure for longer than 15 minutes was found to reduce cell viability. Hence, combining the results of the gel dehydration and cell viability experiments, the wound model was set to receive a single carbon photon treatment for 15 minutes with the light source positioned 20 cm from the wound.

General analysis of wound healing

In this study, we hypothesized that carbon light therapy in combination with a hydrogel dressing would create an ideal extracellular environment for wound healing, and we conducted an *in vivo* study to evaluate the effects and potential mechanisms of this combined treatment. Typically, wounds require the dressing to be changed every 2 days. This study simulated routine clinical procedures by using the same frequency of dressing changes to better provide a reference for clinical work. To determine the healing rate of the wound, we calculated the percentage area of the wound defect (Figure 2c) and recorded typical wound closure images from each group at different time points (Figure 3). Wound healing in the G&C group was more rapid than that

in the other three treatment groups, beginning from 4 days post-wounding. New skin tissue completely filled in the skin defect by 14 days in the G&C group, while wounds were fully healed by 16 days in the CPT group. In the GEL group, wounds had almost completely healed before sacrifice on day 16, while in the BLA group the wounds remained visible and were not well healed by the time of sacrifice. Therefore, the initial data supported the hypothesis that synergistic treatment is beneficial in full-thickness skin wound repair.

Secretion of growth factors related to skin regeneration

TGF-β1 regulates the re-epithelialization process by promoting keratinocyte migration,[18] while VEGF and bFGF are key regulatory growth factors in wound healing, involved in angiogenesis and anti-scar formation.[19] As shown in Figure 4, the secretion of the detected growth factors increased over time during wound healing. At an early stage of wound repair (8 days), the secretion of TGF-β1 from the G&C group was higher than that from the BLA,
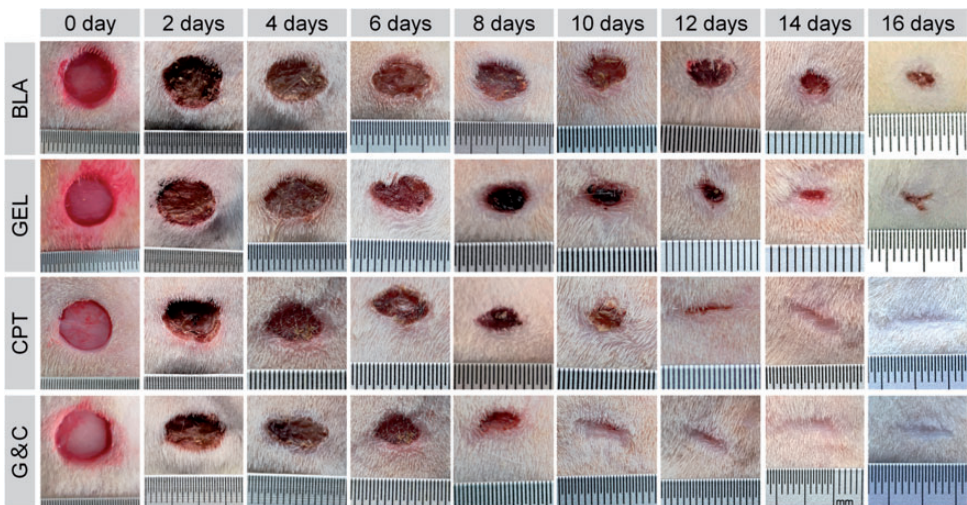

Figure 3. Wound appearances at different timepoints post-wounding in the four treatment groups.
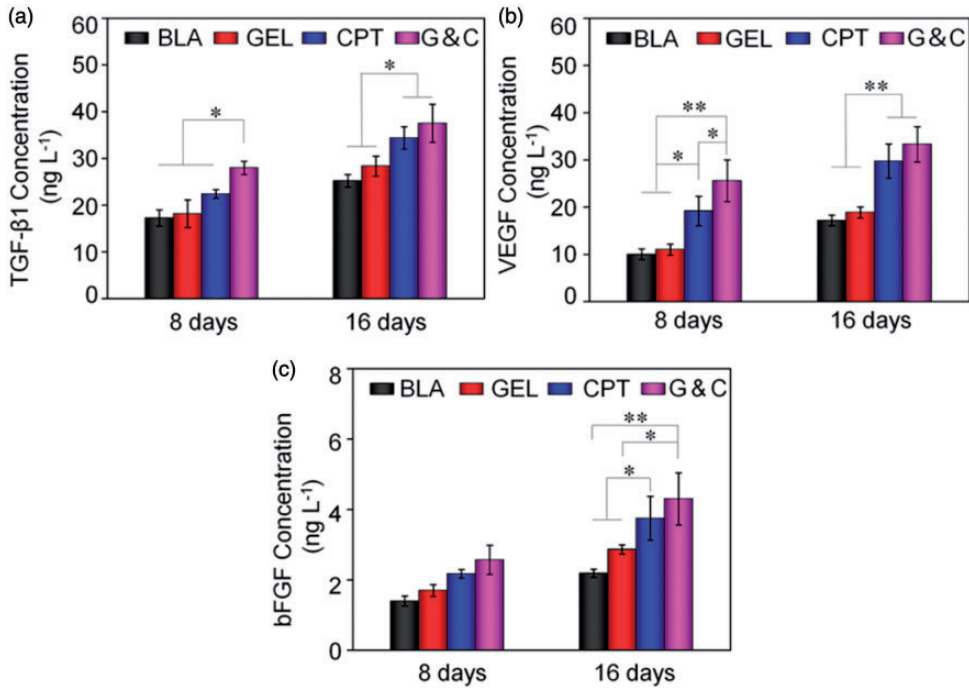
Figure 4. Concentrations of TGF-β1 (a), VEGF (b), and bFGF (c) in regenerated tissue samples from the four experimental groups at 8 and 16 days post wounding. Data represent the mean $\pm$ SD, $n = 3$, *$P < 0.05$, **$P < 0.01$.
TGF, transforming growth factor; VEGF, vascular endothelial growth factor; bFGF, basic fibroblast growth factor.

GEL, and CPT groups ($P < 0.05$ for all vs. G&C; Table 1). Tissue obtained from the G&C group showed the highest level of VEGF expression, with the G&C and CPT groups exhibiting significantly higher VEGF expression than that of the GEL and BLA groups ($P < 0.001$ vs. G&C and $P < 0.05$ vs. CPT). However, the bFGF expression level showed no significant differences between any of the treatment groups. At the late stage of wound repair (16 days), the secretion of TGF-β1 and VEGF in the G&C and CPT groups was significantly higher than that in the BLA and GEL groups ($P < 0.05$ for TGF-β1 and $P < 0.01$ for VEGF). Further, the expression levels of bFGF in the G&C and CPT groups were significantly higher than those in the GEL and BLA groups

($P < 0.001$ to $P < 0.05$ vs. G&C and $P < 0.05$ vs. CPT).

Thus, the differential expression of growth factors in the different treatment groups could be clearly seen. These growth factors were secreted by regenerated tissue and residual skin and appeared to promote the effects of the various treatments tested, especially those of carbon photon therapy. These growth factors may function further as priming factors, thereby leading to enhanced skin healing.[20]

Wound regeneration and maturation

H&E staining and Masson trichrome staining were conducted to observe the progress of epidermal regeneration and inflammatory cell infiltration, as well as scar formation

Table 1. Concentrations of TGF-β1, VEGF, and bFGF in regenerated tissue samples from the four experimental groups at 8 and 16 days post wounding.

Groups	TGF-β1 (ng/L)	VEGF (ng/L)	bFGF (ng/L)
8 days post wounding			
G&C	27.97 ± 1.41[a]	25.52 ± 3.76[b,c]	2.07 ± 0.41
CPT	22.37 ± 0.92	19.23 ± 2.74[d]	1.77 ± 0.12
GEL	18.16 ± 2.97	11.08 ± 1.12	1.70 ± 0.17
BLA	17.25 ± 1.74	10.07 ± 1.04	1.62 ± 0.14
16 days post wounding			
G&C	37.50 ± 4.0[e]	33.67 ± 4.37[f]	4.32 ± 0.73[g,h]
CPT	34.35 ± 2.42[i]	29.80 ± 4.41[j]	3.77 ± 0.65[i]
GEL	28.37 ± 2.13	19.08 ± 2.52	2.87 ± 0.63
BLA	25.19 ± 1.32	17.36 ± 2.61	2.19 ± 0.26

[a]G&C vs. CPT, GEL, and BLA groups, $P < 0.05$; [b]G&C vs. GEL and BLA groups, $P < 0.01$; [c]G&C vs. CPT group, $P < 0.05$; [d]CPT vs. GEL and BLA groups, $P < 0.05$; [e]G&C vs. GEL and BLA groups, $P < 0.05$; [f]G&C vs. GEL and BLA groups, $P < 0.01$; [g]G&C vs. GEL group, $P < 0.05$; [h]G&C vs. BLA group, $P < 0.01$; [i]CPT vs. GEL and BLA groups, $P < 0.05$; [j]CPT vs. GEL and BLA groups, $P < 0.01$. Data represent the mean ± SD, $n = 8$ per group.
TGF, transforming growth factor; VEGF, vascular endothelial growth factor; bFGF, basic fibroblast growth factor.
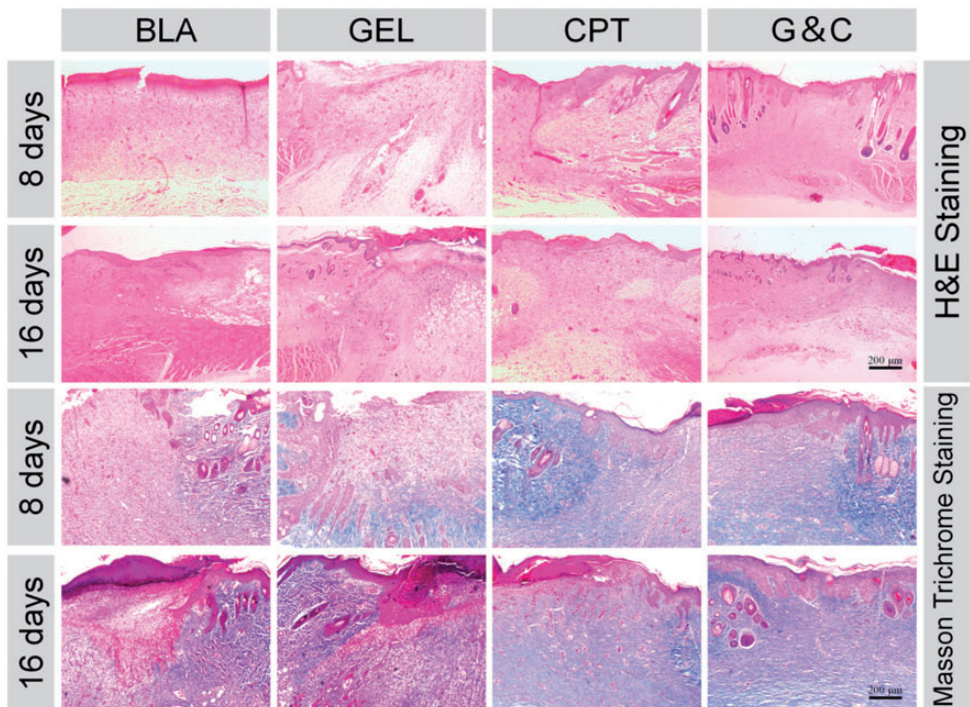

Figure 5. Hematoxylin and eosin (H&E) staining and Masson trichrome staining of regenerated tissue samples from the four treatment groups at days 8 and 16. In the Masson trichrome-stained images, the collagen and nuclei stained blue and black, respectively, while the scar tissue, muscle, cytoplasm, and keratin stained red.
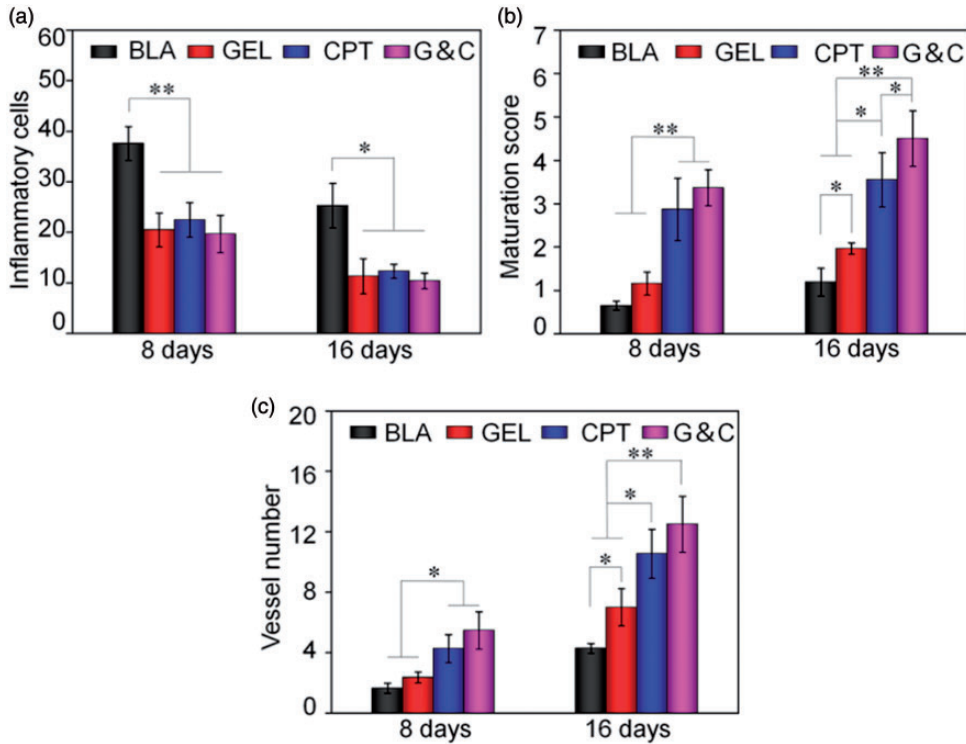
Figure 6. Inflammatory cells (a), maturity score (b), and vessel number (c) in regenerated tissue samples from each treatment group at 8 and 16 days post wounding. Data represent the mean ± SD, $n = 3$, $*P < 0.05$, $**P < 0.01$.

and collagen deposition (Figure 5). On day 8, samples from the G&C group exhibited well-organized granulation tissue at the wound site, while complete healing of the skin defect was observed by 16 days. In contrast, poor granulation was detected in the BLA group at 8 days, with rich granulation tissue formation verified only by 16 days. In the GEL and CPT groups, the formation of granulation tissue was relatively superior to that in the BLA group but inferior to that in the G&C group, particularly at the earlier time point (day 8).

The aggregation and activation of inflammatory cells are important indexes of the inflammatory reflex and infection.[21] Therefore, we quantified inflammatory cell infiltration in tissue samples from the different treatment groups (Figure 6a) and Table 2. The numbers of inflammatory cells at days 8 and 16 in the G&C, CPT, and GEL groups were significantly lower than those in the BLA group ($P < 0.01$ for day 8 and $P < 0.05$ for day 16 vs. BLA).

Collagen deposition has a key role in inhibiting scar formation during wound repair maturation, and wound contraction results from fibroblasts cross-linking with collagen.[22] In this study, the G&C group exhibited the least scar tissue formation and the most collagen deposition, while the CPT group exhibited less scar tissue formation and more collagen deposition than the GEL and BLA groups by both days 8 and 16. The BLA group exhibited minimal collagen deposition and the most scar

Table 2. Numbers of inflammatory cells in regenerated tissue samples from each experimental group at 8 and 16 days post wounding.

Groups	8 days	16 days
G&C	19.68 ± 3.67	10.38 ± 1.56
CPT	22.47 ± 3.39	12.34 ± 1.38
GEL	20.48 ± 3.35	11.31 ± 3.49
BLA	37.60 ± 3.34^{a}	25.27 ± 4.41^{b}

[a]BLA vs. G&C, CPT, and GEL groups, $P < 0.01$; [b]BLA vs. G&C, CPT, and GEL groups, $P < 0.05$. Data represent the mean $\pm$ SD, $n = 8$ per group.

Table 3. Wound maturity scores in regenerated tissue samples from each experimental group at 8 and 16 days post wounding

Groups	8 days	16 days
G&C	3.41 ± 0.49^{a}	$4.48 \pm 0.76^{a,b}$
CPT	2.87 ± 0.79^{c}	3.55 ± 0.72^{c}
GEL	1.16 ± 0.27	1.98 ± 0.17^{d}
BLA	0.64 ± 0.12	1.18 ± 0.26

[a]G&C vs. GEL and BLA groups, $P < 0.01$; [b]G&C vs. CPT group, $P < 0.05$; [c]CPT vs. GEL and BLA groups, $P < 0.05$; [d]GEL vs. BLA group, $P < 0.05$. Data represent the mean $\pm$ SD, $n = 8$ per group.

Table 4. Vessel numbers in regenerated tissue samples from each experimental group at 8 and 16 days post wounding.

Groups	8 days	16 days
G&C	5.47 ± 0.52^{a}	12.55 ± 0.81^{b}
CPT	4.27 ± 0.48^{c}	10.53 ± 0.72^{c}
GEL	2.38 ± 0.23	7.05 ± 0.61^{d}
BLA	1.71 ± 0.29	4.28 ± 0.26

[a]G&C vs. GEL and BLA groups, $P < 0.05$; [b]G&C group vs. GEL and BLA groups, $P < 0.01$; [c]CPT vs. GEL and BLA groups, $P < 0.05$; [d]GEL group vs. BLA group, $P < 0.05$. Data represent the mean $\pm$ SD, $n = 8$ per group.

tissue formation among the treatment groups. According to the wound sub-epithelial dermal matrix maturity scoring system (Figure 6b and Table 3), by both day 8 and 16 the G&C and CPT groups achieved higher maturation scores than those of the GEL and BLA groups, with a significantly higher level of maturation in the G&C group than the CPT group at 16 days ($P < 0.05$); a similar result was observed between the GEL and BLA groups at 16 days ($P < 0.05$).

Keratin formation and neovascularization are also important indexes of wound repair.[23] Hence, K14 and CD31 immuno-histochemical staining were conducted to investigate keratin formation and neovascularization, respectively. First, the vessel numbers in each group were quantified using immunohistochemical staining for CD31 (Figure 6c and Table 4). On day 8, significantly elevated numbers of CD31-positive cells were observed in the G&C and CPT group compared with those in the GEL and BLA groups ($P < 0.05$ vs. both GEL and BLA). By day 16, the number of CD31-positive vessels was highest in the G&C group, indicating superior angiogenesis and blood vessel formation in the granulation tissue ($P < 0.01$). Further, samples from the CPT group exhibited more angiogenesis than those from the GEL and BLA groups ($P < 0.05$). On days 8 and 16, a larger K14-positive area was observed in the G&C group compared with that in the CPT and GEL groups (Figure 7). In addition, the lowest K14 expression level at each time point was observed in the BLA group.

These results may be attributable to the fact that carbon photons can be quickly absorbed by the skin and subcutaneous tissues, which in turn produces thermal and photochemical effects.[24] Carbon photons can also accelerate local blood vessel formation, effectively improving blood microcirculation and tissue nutrition, enhancing the excretion of local exudates, and dissipating inflammation.[25] Further, hydrogel wound dressings can help to seal wounds, reduce infection and scar tissue, and enhance functional tissue regeneration.[26] Taken
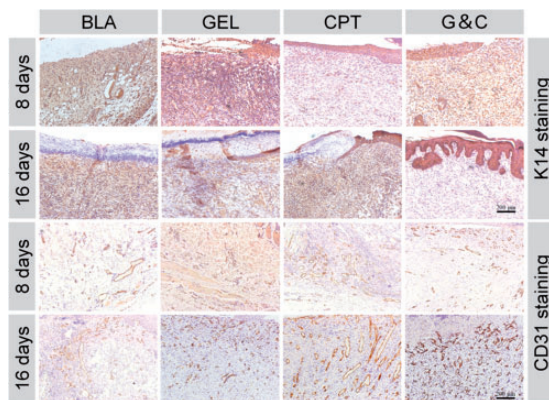
Figure 7. Immunohistochemical staining of K14 and CD31 in regenerated tissue samples from each treatment group at 8 and 16 days post wounding.

together, our findings indicated that synergistic treatment with carbon photon therapy and hydrogel dressing resulted in improved granulation tissue formation, limited inflammatory cell infiltration, improved collagen deposition, and superior neovascularization.

Conclusions

In this study, we verified the wavelength distribution of the light source used for carbon photon therapy, and the safe treatment parameters for carbon photon therapy were selected following *in vitro* experiments. It was demonstrated that the Prontosan hydrogel dressing combined with carbon photon therapy could significantly improve the microenvironment of wound healing in terms of growth factor secretion, granulation tissue formation, inflammation regulation, collagen deposition, and neovascularization. This synergistic treatment provides a new option for wound healing therapy. However, the number of animals in each group was relatively small in this study and a large-scale experimental study is still needed. Further investigation of the in-depth mechanisms and clinical validation thereof are also required.

References

1. Sorg H, Tilkorn DJ, Hager S, et al. Skin wound healing: an update on the current knowledge and concepts. *Eur Surg Res* 2017; 58: 81–94.
2. Han G and Ceilley R. Chronic wound healing: a review of current management and treatments. *Adv Ther* 2017; 34: 599–610.
3. Lemmer B. Light and medicine. *Dtsch Med Wochenschr* 2016; 141: 1840–1844.
4. Buchanan BB. The carbon (formerly dark) reactions of photosynthesis. *Photosynth Res* 2016; 128: 215–217.
5. Yan JX, Liao X, Li SH, et al. Effects of carbon arc lamp irradiation on wound

healing in a rat cutaneous full-thickness wound model. *Photobiomodul Photomed Laser Surg* 2019; 37: 17–24.

6. Okuyama S, Nagaya T, Ogata F, et al. Avoiding thermal injury during near-infrared photoimmunotherapy (NIR-PIT): the importance of NIR light power density. *Oncotarget* 2017; 8: 113194–113201.

7. Liu H, Cheng Y, Wang J, et al. Component effect of stem cell-loaded thermosensitive polypeptide hydrogels on cartilage repair. *Acta Biomater* 2018; 73: 103–111.

8. Liu H, Wang C, Li C, et al. A functional chitosan-based hydrogel as a wound dressing and drug delivery system in the treatment of wound healing. *RSC Adv* 2018; 8: 7533–7549.

9. Bellingeri A, Falciani F, Traspedini P, et al. Effect of a wound cleansing solution on wound bed preparation and inflammation in chronic wounds: a single-blind RCT. *J Wound Care* 2016; 25: 160–168.

10. Wang C, Feng N, Chang F, et al. Injectable cholesterol-enhanced stereocomplex polylactide thermogel loading chondrocytes for optimized cartilage regeneration. *Adv Healthc Mater* 2019; 8: 1900312.

11. Greenhalgh DG, Sprugel KH, Murray MJ, et al. PDGF and FGF stimulate wound healing in the genetically diabetic mouse. *Am J Pathol* 1990; 136: 1235–1246.

12. Lin Z, Li R, Liu Y, et al. Histatin1-modified thiolated chitosan hydrogels enhance wound healing by accelerating cell adhesion, migration and angiogenesis. *Carbohydr Polym* 2020; 230: 115710.

13. Eells JT, Wong-Riley MT, VerHoeve J, et al. Mitochondrial signal transduction in accelerated wound and retinal healing by near-infrared light therapy. *Mitochondrion* 2004; 4: 559–567.

14. Wu SY, Sun YS, Cheng KC, et al. A wound-healing assay based on ultraviolet light ablation. *SLAS Technol* 2017; 22: 36–43.

15. Wu X, Li H and Xiao N. Advancement of near-infrared (NIR) laser interceded surface enactment of proline functionalized graphene oxide with silver nanoparticles for proficient antibacterial, antifungal and wound recuperating therapy in nursing care in hospitals. *J Photochem Photobiol B* 2018; 187: 89–95.

16. Hoque J, Prakash RG, Paramanandham K, et al. Biocompatible injectable hydrogel with potent wound healing and antibacterial properties. *Mol Pharm* 2017; 14: 1218–1230.

17. Li Y, Wang X, Fu YN, et al. Self-adapting hydrogel to improve the therapeutic effect in wound-healing. *ACS Appl Mater Interfaces* 2018; 10: 26046–26055.

18. Bielefeld KA, Amini-Nik S and Alman BA. Cutaneous wound healing: recruiting developmental pathways for regeneration. *Cell Mol Life Sci* 2013; 70: 2059–2081.

19. Hosseinkhani H, Hosseinkhani M, Khademhosseini A, et al. Enhanced angiogenesis through controlled release of basic fibroblast growth factor from peptide amphiphile for tissue regeneration. *Biomaterials* 2006; 27: 5836–5844.

20. Boniakowski AE, Kimball AS, Jacobs BN, et al. Macrophage-mediated inflammation in normal and diabetic wound healing. *J Immunol* 2017; 199: 17–24.

21. Landén NX, Li D and Ståhle M. Transition from inflammation to proliferation: a critical step during wound healing. *Cell Mol Life Sci* 2016; 73: 3861–3885.

22. Felician FF, Yu RH, Li MZ, et al. The wound healing potential of collagen peptides derived from the jellyfish *Rhopilema esculentum*. *Chin J Traumatol* 2019; 22: 12–20.

23. DiPietro LA. Angiogenesis and wound repair: when enough is enough. *J Leukoc Biol* 2016; 100: 979–984.

24. Feng L, Tao D, Dong Z, et al. Near-infrared light activation of quenched liposomal Ce6 for synergistic cancer phototherapy with effective skin protection. *Biomaterials* 2017; 127: 13–24.

25. Keszler A, Lindemer B, Weihrauch D, et al. Red/near infrared light stimulates release of an endothelium dependent vasodilator and rescues vascular dysfunction in a diabetes model. *Free Radic Biol Med* 2017; 113: 157–164.

26. Francesko A, Petkova P and Tzanov T. Hydrogel dressings for advanced wound management. *Curr Med Chem* 2018; 25: 5782–5797.